COBEM 2021 26th International Congress of Mechanical Engineering
November 22-26, 2021, Virtual Congress, Brazil
ABCM Associação Brasileira de Engenharia e Ciências Mecânicas

COB-2021-1019
OPTIMIZATION OF VIBRATION BAND GAPS IN THREE-DIMENSIONAL LATTICE STRUCTURES

Rubens Gonçalves Salsa Junior
Thiago de Paula Sales
Domingos Alves Rade
Aeronautics Institute of Technology, Department of Mechanical Engineering, Pç. Mal. Eduardo Gomes, 50, São José dos Campos, SP 12228-900, Brazil
rsalsa@ita.br, tpsales@ita.br, rade@ita.br

Abstract. *Recent research on structural dynamics has steered towards periodic structures, as band gap phenomena can be explored to mitigate vibration. The main objective of this work is to tackle the optimal design of three-dimensional lattice structures which show one-dimensional periodicity, and incorporate localized resonators to provide band gaps. The unit-cell of the structure was modelled by the Finite Element Method, while band gaps were identified by inspecting the associated dispersion relation, obtained by taking into account Floquet-Bloch boundary conditions. The dependence of the band gaps of the investigated lattice structure on design parameters was duly analyzed. Lastly, the frequency range of band gaps was broadened by casting an optimization problem, which was solved using the differential evolution algorithm. It is shown that the optimized lattice periodic structure can decrease the transmissibility of mechanical waves over a wide range of frequencies, demonstrating its potential utility in diverse applications requiring vibration suppression.*

Keywords: *Phononic crystals, band gaps, resonant metamaterials, optimization, vibration control*

1. INTRODUCTION

An approach to vibration control that has attracted the attention of many researchers involves the use of elastic metamaterials. In structural vibration, elastic metamaterials generally consist of periodic structures, constructed from identical substructures or unit cells, where internal resonances are induced by embedding resonators to the host structure. Elastic metamaterials exhibit properties that are generally viewed to go beyond what one expects to find in naturally occurring or conventional materials. For structural engineering applications, one of the most important features of elastic metamaterials is the possible existence of band gaps, within which the propagation of elastic waves in the structure is prohibited or only evanescent waves with spatial decay exist (Vasileiadis *et al.*, 2021). The manipulation of wave propagation in elastic metamaterials has potential to provide low vibration transmission and high tailorability, without the cost of high-mass structures (Elmadih *et al.*, 2019).

Band gaps can emerge through two different phenomena: Bragg scattering or local resonance. Bragg scattering occurs when the wavelengths of travelling waves become twice the length of the unit cells, so that transmitted and reflected waves within the periodic media undergo destructive interference (Vasileiadis *et al.*, 2021). Because of the dependence on wavelength, which in turn is related to structural stiffness, Bragg band gaps tend to occur at high frequencies in most engineering structures. On the other hand, band gaps associated with local resonances are due to the out-of-phase motion of the base structure with respect to the internal resonators (Baravelli and Ruzzene, 2013), where the energy of elastic waves is absorbed by the resonators (Liu *et al.*, 2000). Additionally, the internal resonant system can be tuned so that band gaps typically materialize at about half the frequencies involved in Bragg phenomena (Hussein *et al.*, 2014). Therefore, elastic metamaterials can leverage the local resonance mechanism between the unit cell and the auxiliary oscillators to ensure a variety of functional improvements with respect to the corresponding resonator-free periodic structure (Bacigalupo *et al.*, 2019).

In this context, researchers have investigated the dispersion properties of three-dimensional lattice structures with internal resonances. This type of structure can be used in architectural and mechanical fields for its high specific stiffness and large surface-to-volume ratio (Zhou *et al.*, 2017), while its band gap properties reveal potential applications in vibration isolation as support structures (Elmadih *et al.*, 2019). Liu *et al.* (2000) proposed the concept of a locally resonant 3D system consisting of lead spheres coated with soft rubber. Wang and Wang (2013) analyzed the mechanism of band gap generation of a 3D holey structure with six-necked and one-necked resonators and investigated the effects of the geometry parameters of the resonators on the band gaps. Matlack *et al.* (2016) embedded steel cubes as local resonators in a polycarbonate beam lattice, and altered the geometrical parameters of the lattice to show a variety of band gap formations due to different local resonant modes. Recently, Elmadih *et al.* (2019) obtained the dispersion relation of a 3D

body centered lattice with reinforced struts. These works show that these types of structures can provide transmissibility reduction of elastic waves, with potential use as support structures, where vibration isolation and impact resistance are essential properties.

While research on these structures focused on obtaining dispersion relations and analyzing the effect of local resonator design parameters on the band gaps width and location, a challenging issue arises when obtaining new configurations that result in wider band gaps in lower frequency ranges. Recently, the optimal design of local resonators has been tackled for some types of structures. Jung *et al.* (2020) used a topology optimization method for designing a local resonator in order to tailor flexural band gaps in plate structures. Bacigalupo *et al.* (2017) combined anti-chiral lattice structure with inertial resonators, and designed the number, arrangements, and material properties of the resonators to improve band gap properties using a nonlinear optimization algorithm. Later, Bacigalupo *et al.* (2019) successfully utilized machine-learning techniques to the spectral optimization of a tetrachiral metamaterial. From the technological viewpoint, a successful optimization of the dispersion properties for elastic metamaterials paves the way for developing a new generation of smart engineering devices (Bacigalupo *et al.*, 2019). In addition, successful implementation of an optimization routine can overcome the difficulties in determining design variables that open up band gaps (Chen *et al.*, 2017). From this perspective, the main objective of this work is to report on a three-dimensional lattice structure which shows one-dimensional periodicity, and incorporates localized resonators optimized to provide wider band gaps in a lower frequency range. The unit cell of the structure was modelled by the Finite Elements Method, while band gaps were identified by inspecting the associated dispersion relation, obtained by taking into account Floquet-Bloch boundary conditions. The dependence of the band gaps of the investigated lattice structure on design parameters was duly analyzed and the mechanism of band gap formation was investigated. Finally, a finite structure is used to validate that the optimized lattice structure can decrease the transmissibility of mechanical waves over a wide range of frequencies, demonstrating its potential utility in diverse applications requiring vibration suppression. The organization is as follows: the structures under investigation and their wave propagation characteristics are expounded in Sect. 2. The optimization methodology and sensitivity analysis are discussed in Sect. 3. Results are shown in Sect. 4. Concluding remarks are listed in Sect. 5.

2. LATTICE STRUCTURE WITH INTERNAL RESONATORS

The 3D lattice structure structure shown in Fig. 1a corresponds to the baseline resonator-free unit cell investigated in this work. It consists of a cubic grid of size L, with outer beams with radius r_o. The inner beams have radius r_i. Inspired by the design of Elmadih *et al.* (2019), a solid sphere of radius r_e is added to the center of the unit cell, as shown in Fig. 1b. This unit cell is conceptualized in a manner so that the sphere and the inner beams can act as a local resonator.

The infinite structure has one-dimensional periodicity along the z direction, as shown in Fig. 1c. For illustration purposes, only the structure with internal resonators is shown. It is assumed that the infinite structure is slender, so that wave propagation is approximately one dimensional, i.e., it is assumed that waves propagate along the z direction. This hypothesis is not at all restrictive since wave modes still involve the standard propagating and evanescent modes, such as longitudinal, bending, torsional and shearing motions.

2.1 Calculation of dispersion relations

The dispersion curves and wave modes of the lattice structures were computed using the Wave Finite Elements (WFE) method. This method is an attractive alternative when modeling complex structures, for which analytical solutions might not be readily available (Waki *et al.*, 2009; Mencik, 2010). In this manner, only the FE model of a unit cell is used, which is combined with Bloch's theorem and Floquet boundary conditions along the interfaces. Consequently, a hybrid approach, that involves computing the mass and stiffness matrices via commercial packages, can be seamlessly implemented (Nobrega *et al.*, 2016). The WFE method is concisely explained as follows. A FE model of a unit cell is constructed and the mass $\mathbf{M}$ and stiffness $\mathbf{K}$ matrices are calculated. For consistency, each boundary along the direction of wave propagation must contain the same number of degrees of freedom (DOFs). The dynamic equilibrium of a unit cell is formulated in the frequency domain as

$$\mathbf{D}\mathbf{q} = \mathbf{f}, \tag{1}$$

where $\mathbf{q}$ and $\mathbf{F}$ represent n-dimensional vectors of generalized displacements and forces, respectively. $\mathbf{D} = \mathbf{K} - \omega^2\mathbf{M}$ represents the $n \times n$ dynamic stiffness operator of a unit cell. The DOFs can be decomposed into internal, left (subscript L) and right (subscript R) boundaries. Assuming that there are no external forces acting on the interior DOFs, Eq. (1) is reformulated in terms of state vectors belonging to the left and right boundaries as

$$\mathbf{u}_R = \mathbf{S}\mathbf{u}_L, \tag{2}$$

where

$$\mathbf{u}_R = \begin{bmatrix} \mathbf{q}_R \\ \mathbf{f}_R \end{bmatrix} \qquad \text{and} \qquad \mathbf{u}_L = \begin{bmatrix} \mathbf{q}_L \\ -\mathbf{f}_L \end{bmatrix}. \tag{3}$$

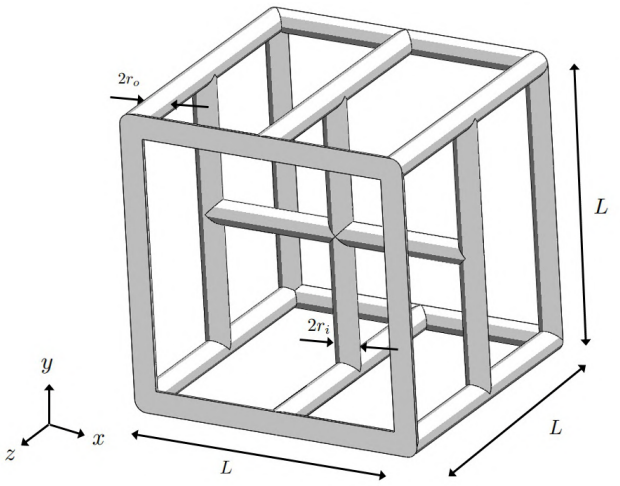

(a) Schematic of resonator-free unit cell.

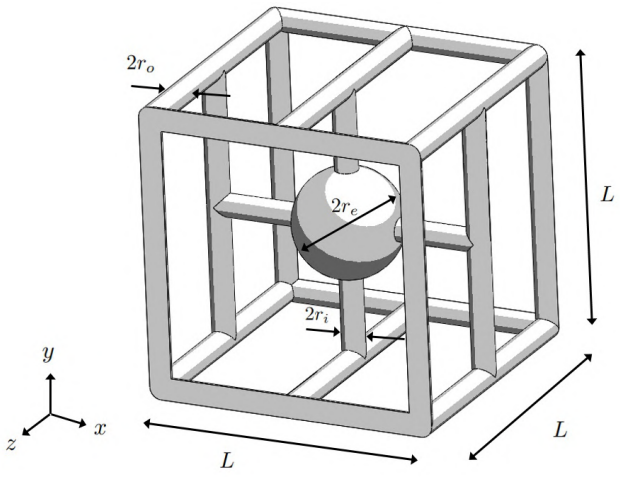

(b) Schematic of unit cell with resonator.

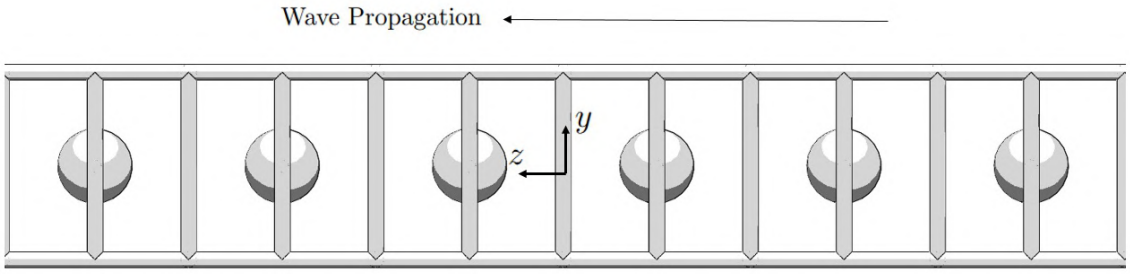

(c) One-dimensional wave propagation in the infinite structure.

Figure 1: Unit cells of length L. The outer beams have radius r_o and inner beams have radius r_i. The sphere has radius r_e.

Here, $\mathbf{S}$ is a $2n \times 2n$ symplectic matrix composed of sub-blocks of the dynamic stiffness matrix condensed onto its left and right boundaries. Periodicity along the propagation direction implies the coupling condition between two consecutive unit cells k and $k-1$, i.e.:

$$\mathbf{u}_L^{(k)} = \mathbf{u}_R^{(k-1)}. \tag{4}$$

This condition, combined with Eq. (2), yields

$$\mathbf{u}_L^{(k)} = \mathbf{S}\mathbf{u}_L^{(k-1)}. \tag{5}$$

The solutions of Eq. (5) must be of the form $\mathbf{u}_L^{(k)} = \mu \mathbf{u}_L^{(k-1)}$, according to Bloch's theorem. They are computed by solving the eigenvalue problem

$$\mathbf{S}\mathbf{\Phi} = \mu\mathbf{\Phi}. \tag{6}$$

The scalar parameter μ is related to the wave number k through the relation

$$\mu = e^{-ikL}, \tag{7}$$

while the corresponding $2n$-dimensional vector $\mathbf{\Phi}$ gathers information concerning the wave mode shape, related to the spatial distribution of the displacements and internal forces over the cross-section of the unit cell along its boundaries. Here, L is the length of the unit cell in the direction of wave propagation. The imaginary part of the wave numbers k is related to the spacial decay of the corresponding wave mode. Therefore, for purely propagating waves, k must be real. From the dispersion relations $k(\omega)$, the band gaps, in which waves cannot propagate freely, can be readily identified for an infinite periodic structure.

2.2 Initial design and FE model

The unit cell is initially designed with the dimensions $L = 10$ mm, $r_o = 0.42$ mm, $r_i = 0.42$ mm, $r_e = 2$ mm. It is also assumed its material is structural steel, with density $\rho = 7850$ kg/m^3, Poisson ratio $\nu = 0.3$, and Young's modulus $E = 200$ GPa.

Initially, the unit cell was discretized with 3D quadratic tetrahedral elements, but exorbitant computational costs in simulations lead to a simplified model. The simplified beam-sphere model adopts Timoshenko beam FEs (which capture shear-deformation effects), as well as a solid rigid body to model the sphere at the center of the unit cell. Fig. 2 shows that the smallest natural frequencies of the unit cells, when computed for the two models and considering free boundary conditions, show similar trends. The natural frequencies differ by 10.7% in average for the models with local resonator and 12.6% for the models without resonator.

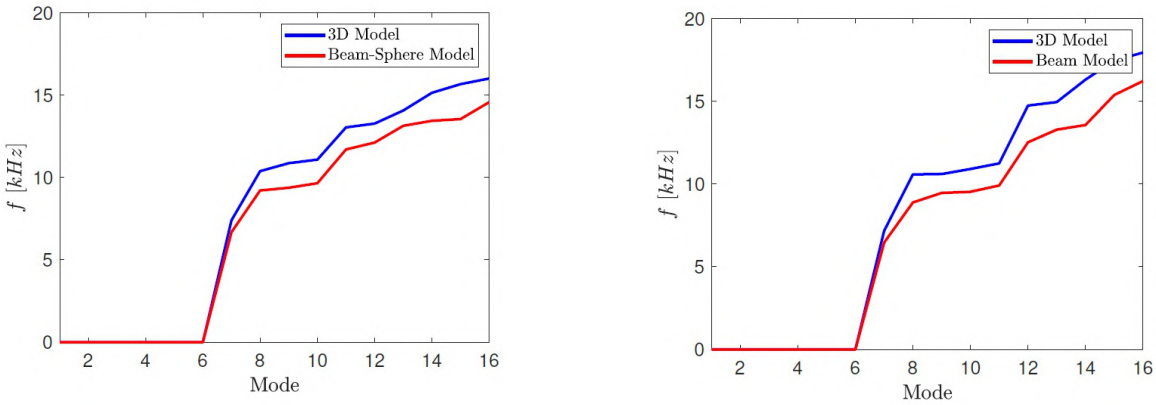

(a) FE models with local resonator.

(b) FE models without resonator.

Figure 2: Smallest natural frequencies for 3D models and simplified, beam FE-based models.

Fig. 3 compares the dispersion relation for propagating wave modes computed with the two models. The dispersion curves for the structure with internal local-resonators (Fig. 3a) and the resonator-free structure (Fig. 3b) were computed with the WFE method. Besides small differences expected due to the nature of both models, the diagrams show similar behavior of wave modes. Therefore, the simplified model is justified. It should be noted that the structures do not have complete band gaps in the frequency range shown, suggesting that an optimization problem could be posed in order to open up and maximize band gaps.

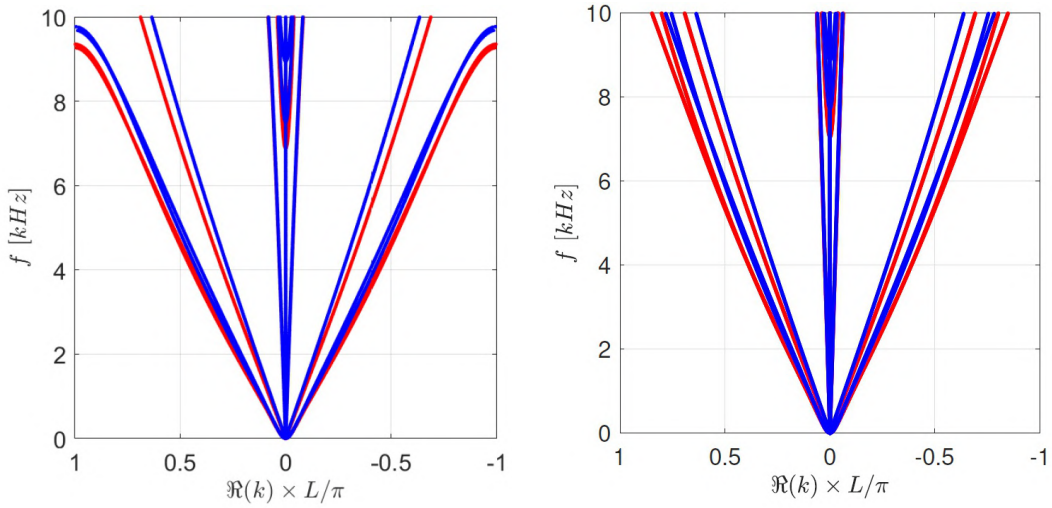

(a) FE models with local resonator.

(b) FE models without resonator.

Figure 3: Comparison of dispersion diagrams for the initial design of the lattice structures obtained with the 3D FE model using quadratic tetrahedral solid elements (•) and the simplified Timoshenko beam model (•).

The four wave modes propagating at 2 kHz are shown in Fig. 4 for both structures. There are two bending wave modes (with respect to axes x and y), a longitudinal wave mode along z, and a torsional mode. A complete band gap must extinguish propagation of these four modes.

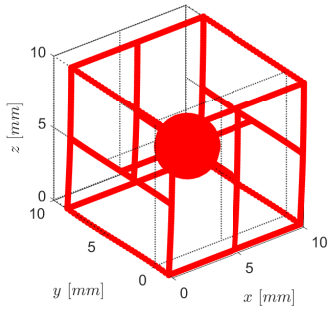

(a) First bending wave mode for structure with resonator.

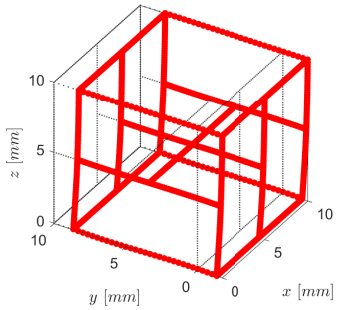

(b) First bending wave mode for resonator-free structure.

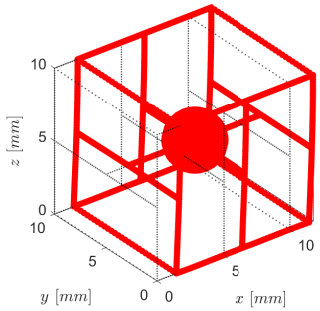

(c) Second bending wave mode for structure with resonator.

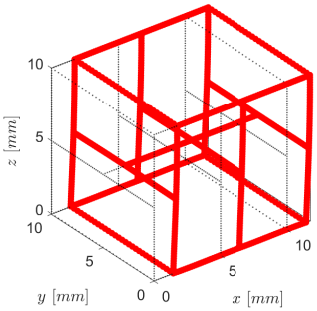

(d) Second bending wave mode for resonator-free structure.

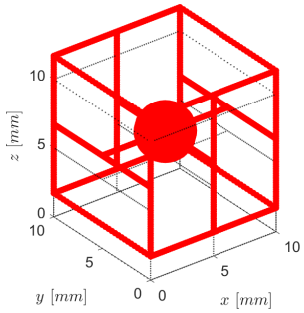

(e) Longitudinal wave mode for structure with resonator.

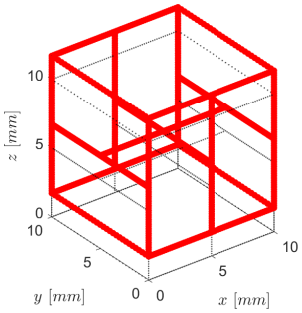

(f) Longitudinal wave mode for resonator-free structure.

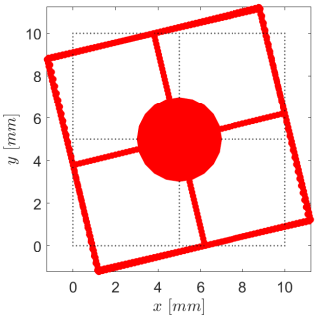

(g) Torsional wave mode for structure with resonator.

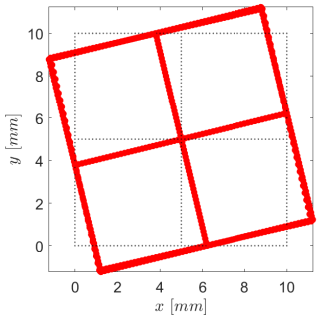

(h) Torsional wave mode for resonator-free structure.

Figure 4: Wave modes at $f = 2$ kHz plotted as nodal displacements. The unit cell is plotted in gray and displaced cell is plotted in red.

3. OPTIMIZATION

3.1 Parametric analysis of band gap formation

The design parameters chosen for band gap optimization are those directly linked with the internal oscillator, composed of the rigid sphere and internal elastic beams attached to the sphere. In particular, the radius of the internal beams, r_i,

and the radius of the sphere, r_e, were considered as the two design variables. It should be noted that there is coupling between the radius of the sphere and the stiffness provided by the internal beams, since their length is directly impacted by the presence of the sphere. Other parameters could have been chosen as well, such as mass density or Young's modulus. However, attention has been restricted to geometric parameters of the resonator to represent cases where ease of manufacturability is desirable.

The interest is to appraise how r_i and r_e affect the band gap formation. Fig. 5 shows the location of complete band gaps for different values of r_i and r_e, i.e., band gaps that encapsulates all wave modes simultaneously. These correspond to regions where the all wave numbers have null real part (non-propagating waves). Firstly, the radius of the sphere is assumed to be given by $r_e = 3.766$ mm, while r_i is varied $(0,\ 0.42]$ mm. This upper limit is equal to the radius r_o of the outer beams. The constant value of r_e is arbitrarily chosen, with the restriction that band gaps can be observed when r_i is swept in the investigated frequency range. It is shown that the band gap is the widest for an intermediate value of r_i. Furthermore, increasing or decreasing the value of r_i shifts the band gap to the right or left, respectively, and it becomes narrower, until no band gap is observed (not shown in the figure).

Similarly, the radius of the internal beams was also held constant, $r_i = 0.145$ mm, while r_e was varied within the range $(0,\ 4]$ mm. Now, this upper limit is imposed as a size restriction, since the edges of the unit cell have length $L = 10$ mm. Fig. 5 shows that band gaps are wider for larger values of r_e, and that the band gap frequency range is shifted to the right. It is also interesting to note that, if r_e is not large enough, band gaps might not appear at all.

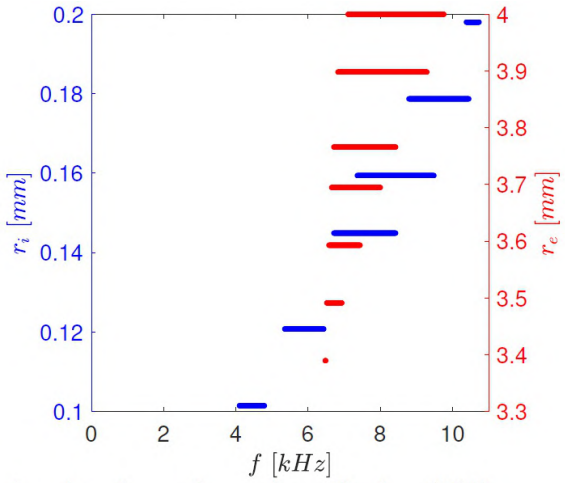

Figure 5: Parametric analysis of complete band gap formation. Each solid line represents the frequency span of a band gap, where all wave numbers have null real part. Red lines are associated with the axis on the right, and are obtained by varying r_e, taking $r_i = 0.145$ mm. Blue lines are associated with the axis on the left, and are obtained by varying r_i, assuming $r_e = 3.766$ mm.

3.2 Optimization problem definition

To obtain a band gap that is the widest and occurs at the lowest possible frequency range, geometric design parameters can be determined by formulating an appropriate optimization problem. In a similar setting, success has been achieved by Han and Zhang (2019) and Poggetto and Arruda (2021) through the use of an objective function that involves the ratio between the the band gap mean frequency and its width, which is the strategy adopted here:

$$\min_{r_i, r_e} f_{obj} = \min_{r_i, r_e} \frac{(\omega_u + \omega_l)/2}{\omega_u - \omega_l}, \tag{8}$$

where ω_l is the lower frequency limit of a band gap and ω_u is the upper frequency limit. This minimization problem has been numerically solved using the Differential Evolution (DE) method, which has emerged as one of the most frequently used algorithms for solving complex optimization problems (Pant *et al.*, 2020). It is a meta-heuristic technique that follows the concepts of the theory of the evolution of species and can be separated in two phases: initialization and evolution. In the first phase, a set of N uniformly distributed population members is generated randomly in the search space. In the next phase, the generated population undergoes mutation, crossover and selection processes. It should be noted that the dispersion relation is computed with the WFE method for each new population member created. This process is repeated until a termination criteria is met. If the optimization is carried in the frequency interval $[\omega_1, \omega_2]$, the termination criteria is that either $\omega_l = \omega_1$ and $\omega_u = \omega_2$, or that the best and worst solutions found in a population be the same. A procedure is implemented as well, in which population members that do not possess band gaps are associated with $f_{obj} \to \infty$.

4. RESULTS

During the optimization, the radius of the internal beams was restricted to lie in the range $r_i \in (0, 0.42]$ mm, where the upper limit 0.42 mm represents the radius of the outer beams. The radius of the sphere is restricted to lie in $r_e \in (0, 4]$ mm. The upper limit of 4 mm is due to size constraints, since the edges of the unit cell have length $L = 10$ mm.

The algorithm was initialized with $N = 20$ population members and the frequency range analyzed is $0 - 10$ kHz, discretized in steps of 5 Hz. Due to the heuristic nature of the employed optimization methodology, 10 runs were performed, and the best solution among them (smallest value of f_{obj}) was taken to be the optimal one. The algorithm terminated its run after 152 generations. The optimal values found are $r_i = 0.132$ mm and $r_e = 4$ mm, and Fig. 6 shows the corresponding dispersion relation for the optimal periodic structure with local resonators. It is shown that no elastic waves can propagated in the range $6360 - 9006$ Hz, which characterizes a complete band gap for all wave modes. Partial band gaps for specific wave types can be wider because they start at lower frequencies. For example, the band gaps for the two bending wave modes start at 3585 Hz and 3645 Hz. Similarly, the band gap for the longitudinal wave mode starts at 4202 Hz. The effect of the resonator is also evidenced when comparing this dispersion relation with that of the resonator-free structure, as shown in Fig. 6. The resonator-free structure possess no band gaps in the frequency region shown.

It is clear that the optimized structure has increased mass when compared to the originally designed unit cell: the initial design had mass of 8.063 g, while the optimized resonant structure has 26.023 g. This evidences the fact that the inertia of the oscillator has to be increased in order to amplify its effectiveness in lowest frequency range possible and generate the widest band gap. This solution might not be applicable to instances when there is a constraint on added mass.

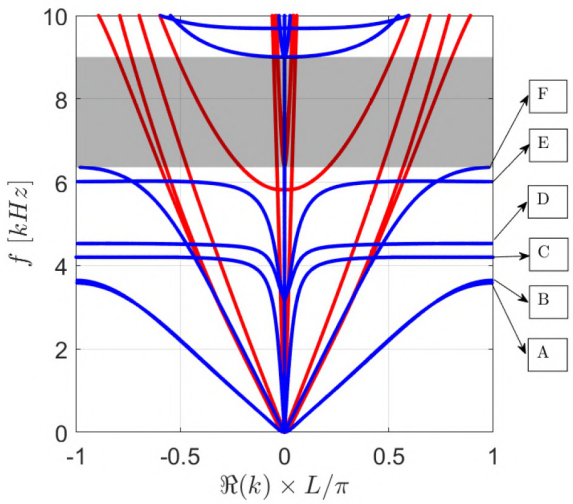

Figure 6: Dispersion curves for periodic structure with local resonators (●) and resonator-free lattice structure (●) with optimal dimensions for the resonator. Complete band gap for the optimal meta-structure is marked with a shaded area.

In order to investigate the mechanism of band gap formation, the band gap opening modes, labeled A-F in Fig. 6, are plotted in Fig. 7. To serve as a reference, the undeformed unit cell is outlined in black. It can be observed that, in modes A-C, the resonator vibrates out-of-phase with respect to the outer beam structure. At the same time, the oscillator vibrates profusely while the outer beam structure is comparatively vibrationless in modes D-F. These represent typical behavior of locally resonant elastic systems (Baravelli and Ruzzene, 2013; Liu *et al.*, 2000; Zhang *et al.*, 2015).

The results of the optimization are now validated for a finite structure composed of 20 unit cells, such as the one shown in Fig. 8 (resonator-free configuration). No geometrical restrictions are imposed at this stage (free boundary conditions). Different harmonic base motions are imposed on the left interface of the structure and the corresponding transmitted displacement is measure for the point indicated at the right interface. For example, if a base motion is imposed along y, then the y component of the displacement is measured for that point, and so on for x and z components. The torsional transmissibility, in particular, was calculated by imposing a rotation of the left interface about the z axis, and the corresponding rotation was measured for the indicated point at the right interface.

Fig. 9a depicts the transmissibility for bending motion along the y axis. The dispersion relation indicates that the band gap for this mode starts at 3585 Hz, which is roughly the value indicated in the transmissibility plot. A similar situation arises when analyzing the transmissibility result for the bending motion along x and for the longitudinal motion (along z), shown in Figs. 9b and 9c, respectively. Since the torsional wave mode was the last to open up a band gap, the region of reduced transmissibility is narrow, as indicated in Fig. 9d.

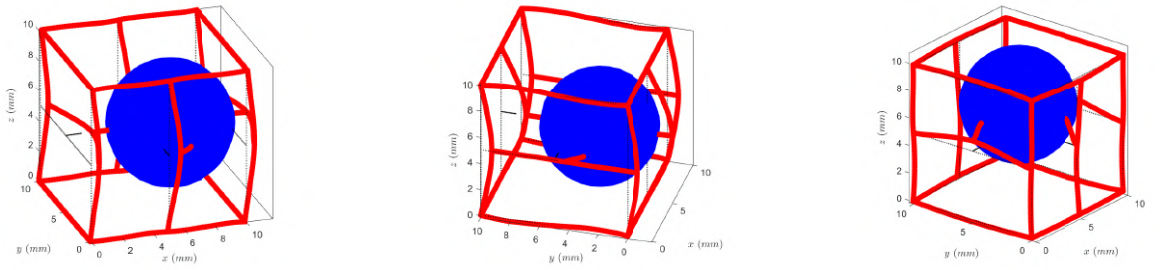

(a) Wave mode at point A. (b) Wave mode at point B. (c) Wave mode at point C.

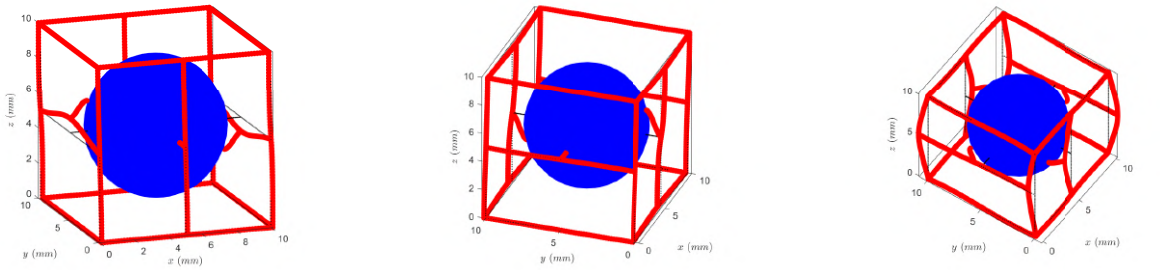

(d) Wave mode at point D. (e) Wave mode at point E. (f) Wave mode at point F.

Figure 7: Wave modes at the lower boundaries of band gaps, plotted as nodal displacements. The sphere is plotted in blue to facilitate visualization. Refer to Fig. 6 for labels A-F.

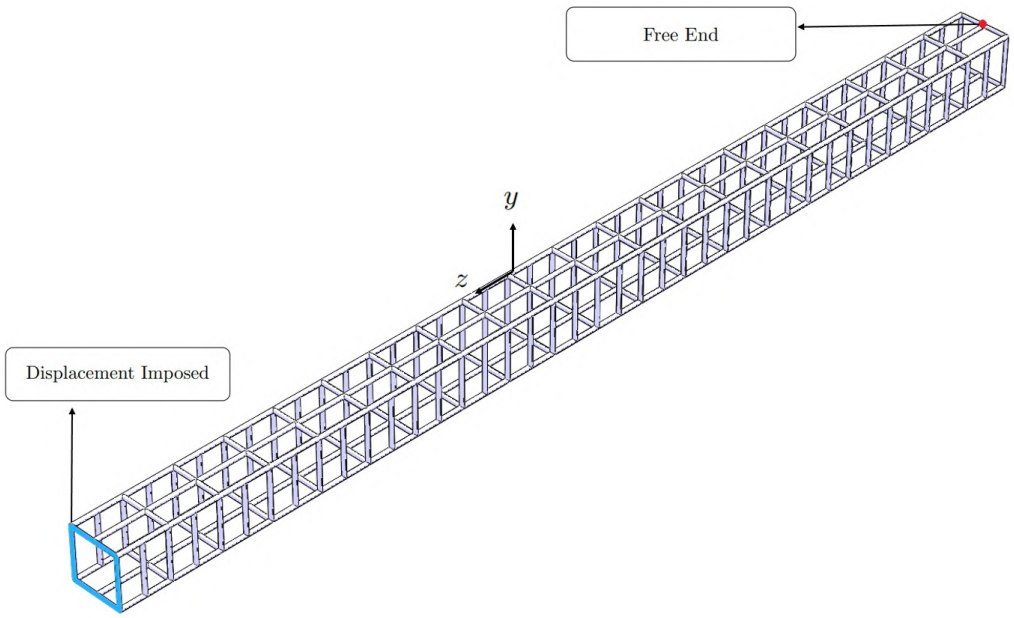

Figure 8: Finite structure with 20 unit cells. Displacements are imposed on the left and transmitted motion is measured on the point indicated at the right (free) end.

5. CONCLUSIONS

A three-dimensional lattice structure which shows one-dimensional periodicity and incorporates localized resonators has been investigated. It was shown how the band gaps depend on the parameters of the local resonators, specifically the radius of the supporting beams and the radius of the sphere. The localized resonators were successfully optimized by a differential evolution algorithm to provide wider band gaps in a lower frequency range. The formation mechanism of the local resonant band gaps was clarified. Finally, the optimal result was validated by considering the response of a finite structure: the transmissibility of bending, longitudinal and torsional waves decrease over a wide range of frequencies,

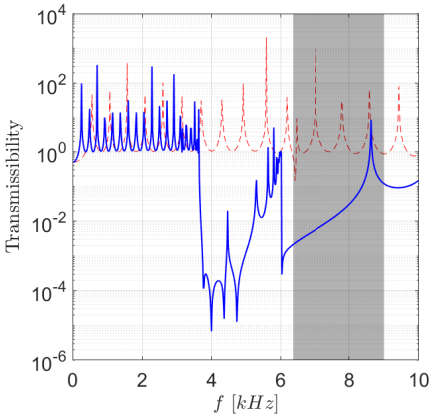

(a) Bending along y axis.

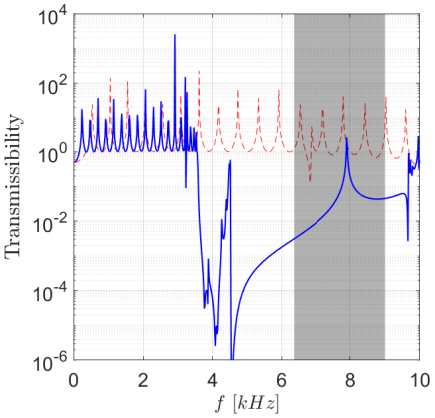

(b) Bending along x axis.

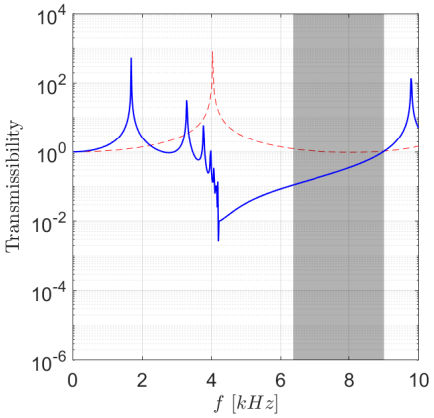

(c) Longitudinal motion.

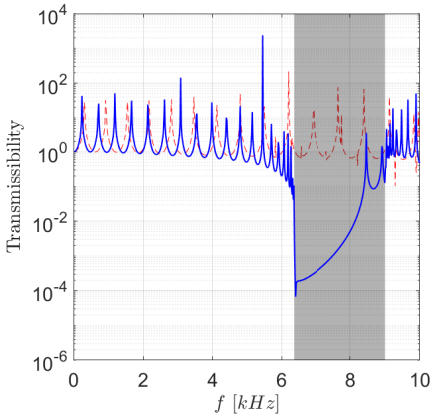

(d) Torsional motion.

Figure 9: Transmissibility of different displacement modes for finite structures made up of 20 unit cells. The plots show comparisons between the structure with localized resonators (—) and its resonator-free counterpart (- -). The shaded area indicates the predicted complete band gap.

demonstrating potential utility in diverse applications requiring vibration suppression.

6. ACKNOWLEDGEMENTS

Authors would like to acknowledge the financial support provided by the São Paulo Research Foundation (FAPESP, grants #2018/15894-0 and #2020/06022-0). D.A. Rade acknowledges the Brazilian Research Council (CNPq) (grants #310633/2013-3 and #312068/2020-4).

7. REFERENCES

Bacigalupo, A., Gnecco, G., Lepidi, M. and Gambarotta, L., 2017. "Optimal design of low-frequency band gaps in anti-tetrachiral lattice meta-materials". *Composites Part B: Engineering*, Vol. 115, pp. 341–359.

Bacigalupo, A., Gnecco, G., Lepidi, M. and Gambarotta, L., 2019. "Machine-learning techniques for the optimal design of acoustic metamaterials". *Journal of Optimization Theory and Applications*, pp. 1–24.

Baravelli, E. and Ruzzene, M., 2013. "Internally resonating lattices for bandgap generation and low-frequency vibration control". *Journal of Sound and Vibration*, Vol. 332, No. 25, pp. 6562–6579.

Chen, Y., Huang, X., Sun, G., Yan, X. and Li, G., 2017. "Maximizing spatial decay of evanescent waves in phononic crystals by topology optimization". *Computers & Structures*, Vol. 182, pp. 430–447.

Elmadih, W., Syam, W.P., Maskery, I., Chronopoulos, D. and Leach, R., 2019. "Multidimensional phononic bandgaps in three-dimensional lattices for additive manufacturing". *Materials*, Vol. 12, No. 11, p. 1878.

Han, X. and Zhang, Z., 2019. "Topological optimization of phononic crystal thin plate by a genetic algorithm". *Scientific reports*, Vol. 9, No. 1, pp. 1–13.

Hussein, M.I., Leamy, M.J. and Ruzzene, M., 2014. "Dynamics of Phononic Materials and Structures: Historical Origins, Recent Progress, and Future Outlook". *Applied Mechanics Reviews*, Vol. 66, No. 4.

Jung, J., Goo, S. and Kook, J., 2020. "Design of a local resonator using topology optimization to tailor bandgaps in plate structures". *Materials & Design*, Vol. 191, p. 108627.

Liu, Z., Zhang, X., Mao, Y., Zhu, Y.Y., Yang, Z., Chan, C.T. and Sheng, P., 2000. "Locally resonant sonic materials". *Science*, Vol. 289, No. 5485, pp. 1734–1736.

Matlack, K.H., Bauhofer, A., Krödel, S., Palermo, A. and Daraio, C., 2016. "Composite 3d-printed metastructures for low-frequency and broadband vibration absorption". *Proceedings of the National Academy of Sciences*, Vol. 113, No. 30, pp. 8386–8390.

Mencik, J.M., 2010. "On the low-and mid-frequency forced response of elastic structures using wave finite elements with one-dimensional propagation". *Computers & Structures*, Vol. 88, No. 11-12, pp. 674–689.

Nobrega, E.D., Gautier, F., Pelat, A. and Dos Santos, J.M.C., 2016. "Vibration band gaps for elastic metamaterial rods using wave finite element method". *Mechanical Systems and Signal Processing*, Vol. 79, pp. 192–202.

Pant, M., Zaheer, H., Garcia-Hernandez, L., Abraham, A. *et al.*, 2020. "Differential evolution: a review of more than two decades of research". *Engineering Applications of Artificial Intelligence*, Vol. 90, p. 103479.

Poggetto, V.F. and Arruda, J.R.F., 2021. "Widening wave band gaps of periodic plates via shape optimization using spatial fourier coefficients". *Mechanical Systems and Signal Processing*, Vol. 147, p. 107098.

Vasileiadis, T., Varghese, J., Babacic, V., Gomis-Bresco, J., Navarro Urrios, D. and Graczykowski, B., 2021. "Progress and perspectives on phononic crystals". *Journal of Applied Physics*, Vol. 129, No. 16, p. 160901.

Waki, Y., Mace, B. and Brennan, M., 2009. "Numerical issues concerning the wave and finite element method for free and forced vibrations of waveguides". *Journal of Sound and Vibration*, Vol. 327, No. 1-2, pp. 92–108.

Wang, Y.F. and Wang, Y.S., 2013. "Complete Bandgap in Three-Dimensional Holey Phononic Crystals With Resonators". *Journal of Vibration and Acoustics*, Vol. 135, No. 4.

Zhang, H., Xiao, Y., Wen, J., Yu, D. and Wen, X., 2015. "Flexural wave band gaps in metamaterial beams with membrane-type resonators: Theory and experiment". *Journal of Physics D: Applied Physics*, Vol. 48, No. 43, p. 435305.

Zhou, X., Wang, J., Wang, R. and Lin, J., 2017. "Band gaps in grid structure with periodic local resonator subsystems". *Modern Physics Letters B*, Vol. 31, No. 25, p. 1750225.

8. RESPONSIBILITY NOTICE

The authors are solely responsible for the printed material included in this paper.